Measurement of Coordinates for a Cylindrical Target Using Times of Flight from a 1-Transmitter and 4-Receiver UWB Antenna System

Gennadiy P. Pochanin, *Senior Member, IEEE*, Lorenzo Capineri, *Senior Member, IEEE*, Timothy D. Bechtel, *Member, IEEE*, P. Falorni, Giovanni Borgioli, Vadym P. Ruban, *Member, IEEE*, Oleksandr A. Orlenko, Tetiana M. Ogurtsova, Oleksandr G. Pochanin, Fronefield Crawford, P. Kholod, and L. Bossi

***Abstract*— This article presents a new UWB impulse radar system consisting of a central radiating antenna (1.9-GHz center frequency, 2-GHz bandwidth) and four receiving antennas designed for the detection and location of dielectrically large objects with dimensions comparable to the spatial dimensions of the probe pulse. Together with the radar system, a solution method for determining the coordinates for detected targets is developed based on the time of flight (TOF) of the probing pulse along raypaths from the radiating antenna to the object, and then reflected to each of the receiving antennas. An algorithm based on the Pearson's correlation coefficient is used to accurately determine the TOF of the signals scattered by the object. The antenna geometry makes it possible to use simple trigonometry and Heron's formula, to calculate the coordinates of the reflecting bright spot on a target. The algorithm has been tested by numerical simulations and experiments with a cylindrical metallic object (diameter 10 cm) and a plastic-cased PMN-2 landmine buried in natural clay soil. For the experiment, GPR signals were acquired on a 4 × 4 square grid at 10-cm step from a height of about 30 cm above the ground. The system detected the test object in all positions and the positioning error in majority is equivalent to the object size.**

***Index Terms*— Antenna system, Heron's formula, humanitarian demining, landmine, Pearson's correlation, target location, time of flight (TOF), UWB impulse radar.**

Manuscript received June 27, 2018; revised November 19, 2018, April 20, 2019, July 9, 2019, and October 4, 2019; accepted October 4, 2019. Date of publication October 21, 2019; date of current version January 21, 2020. This work was supported by the North Atlantic Treaty Organization (NATO) Science for Peace and Security Programme "Holographic and Impulse Subsurface Radar for Landmine and Improvised Explosive Device (IED) Detection," under Grant #G5014. *(Corresponding author: Lorenzo Capineri.)*

G. P. Pochanin, V. Ruban, O. A. Orlenko, T. M. Ogurtsova, O. G. Pochanin, and P. Kholod are with the O.Ya. Usikov Institute for Radiophysics and Electronics of the National Academy of Sciences of Ukraine, 61085 Kharkiv, Ukraine (e-mail: gpp@ire.kharkov.ua).

L. Capineri, P. Falorni, and L. Bossi are with the Department of Information Engineering, University of Florence, 50139 Florence, Italy (e-mail: capineri@ieee.org).

T. D. Bechtel and F. Crawford are with the Franklin and Marshall College, Lancaster, PA 17603 USA (e-mail: tbechtel@fandm.edu).

G. Borgioli is with the Department of Mathematic and Informatic "U. Dini," University of Florence, 50139 Florence, Italy (e-mail: lorenzo.capineri@unifi.it).

This article has supplementary downloadable material available at http://ieeexplore.ieee.org, provided by the authors.

Color versions of one or more of the figures in this article are available online at http://ieeexplore.ieee.org.

Digital Object Identifier 10.1109/TGRS.2019.2946064

I. Introduction

As part of the construction of a low-cost robotic landmine detection vehicle carrying multiple sensors—including ground-penetrating radar (GPR) [1]–[8], we have developed a novel one-transmitter and four-receiver (1 Tx + 4 Rx) UWB antenna array that is cantilever-mounted ahead of the robotic platform as shown in Fig. 1. This impulse GPR system was specifically designed for rapid detection of subsurface mine-like targets [9]. With four receivers, it is possible to obtain the coordinates (x, y, z) of the effective reflection point or bright spot on the target. Upon initial detection of a strong reflection, the robot automatically halts, and the time of flight (TOF) data for each receiver are used to determine the target coordinates. Following this detection and localization, holographic subsurface imaging radar and a 3-D TOF camera will identify and classify the detected target as possible mine or harmless clutter as described in [10] and [11]. This article focuses on the algorithm for determining target location. The antennae and the allied system design and integration are described in concurrent [12], [13] and future works.

This article is organized as follows. In Section II, the proposed target detection and discrimination strategy is outlined, and in Section III, the algorithm for object detection is detailed, followed by the TOF measurements method in Section IV. Finally, Section V presents experimental validation of the method and discussion of the results.

II. 1 Tx + 4 Rx Antenna System

The antenna system is shown schematically in Fig. 1, mounted ahead of the robotic platform. Overlain on this rendering is the local Cartesian coordinate system. M is a cylindrical landmine (see gray disk in Fig. 1). To perform the search phase, the robot advances under remote control along Y. Initially, we assume that the top of M is flush with the ground surface. This assumption is shown (in Section V) to be valid for mine-like objects at typical shallow depths less than 10 cm [14]. This specific reference system simplifies and is validated by the analysis of real radar data later in this article.

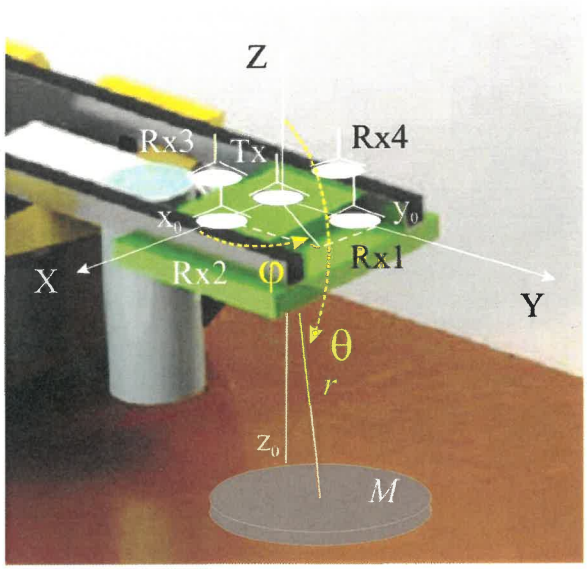

Fig. 1. Schematic of the 1 Tx + 4 Rx UWB antenna system and geometric parameters. The 1 Tx + 4 Rx UWB antenna system is housed in the green case. Light gray cylinder: holographic radar for target discrimination.

In the adopted reference system, the possible object coordinates satisfy the following conditions:

$$-\infty \le x \le +\infty \tag{1}$$

$$y \ge Y_{\min} \tag{2}$$

$$z \le 0 \tag{3}$$

where $Y_{\min}$ is the minimum y coordinate before which the object must be detected. Assume that the system can detect targets without errors ahead of T_x (y is positive). This means that $Y_{\min} = 0$. By constraining y to positive values, we assume that as the robot moves along a survey lane, any "new" object can appear only in the lower front quarter of the coordinate space. That is, no objects of interest are located above the antenna system (e.g., spurious overhead reflections), and no objects of interest are located under or behind the robotic platform (e.g., spurious reflections from the vehicle itself). The intention is to minimize false positive detections and provide a factor-of-safety in the automatic halting of the vehicle by classifying reflections as possible targets before the x-axis crosses the position of the object. This also allows exclusion of false positive detections related to the measurement errors in the TOF data as described in Section V. Note that here, false positive refers only to mistakenly classifying a phantom as a real target. Discrimination of mines from clutter is not the task of the 1 Tx + 4 Rx impulse GPR; that is accomplished with a holographic radar as described in [11].

III. Geometrical Approach Based on Heron's Formula

We can consider the whole antenna system as two independent arrays, each consisting of the transmitter and two receiving antennae. Each array defines one of the local horizontal coordinate axes. For each part, we can independently solve for target location within a two-dimensional plane containing the two Rx antennae and the target M (Fig. 2). Although these planes also contain Tx, we will distinguish them by naming one plane Rx2-*M*-Rx4 and the other Rx1-*M*-Rx3.

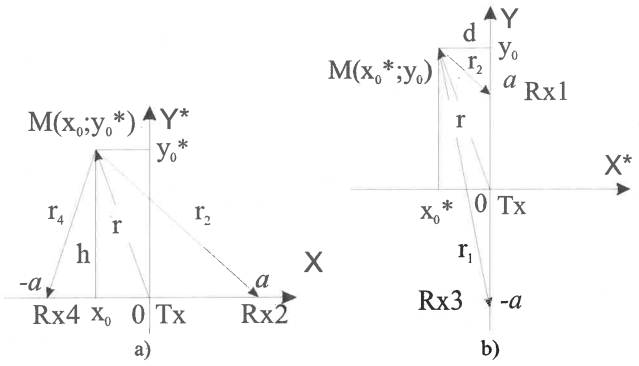

Fig. 2. Coordinate systems and geometric parameters for (a) Rx2-M-Rx4 plane and (b) Rx1-M-Rx3. The coordinates y_0^* and x_0^* may not be the same as y_0 and x_0 in Fig. 1 because the considered planes are not horizontal.

For the sake of completeness, we report the full mathematical details leading to the solutions for the planes Rx2, Rx4, and M (and Tx) and Rx1, Rx3, and M (and Tx). The two solutions in terms of measured TOFs (t_1, t_2, t_3, t_4), v and a, are reported in (18)–(20) and (34)–(36), respectively.

A. Solution in the Plane Rx2-M-Rx4

Consider the plane containing Rx2, Rx4, and M (and Tx). Rx2 and Rx4 are symmetrical with respect to the origin at a distance a [see Fig. 2(a)]. For the solution in this plane, we use the coordinate $y*$ which may not match the local reference system in Fig. 1 because this plane is not horizontal. The known parameters in this calculation are the TOFs for signals along the paths Tx-*M*-Rx2 and Tx-*M*-Rx4. These TOFs are designated t_2 and t_4, respectively. The speed of the electromagnetic wave propagation is v. The immediate task is determination of the coordinates for object M in this plane (x_0, y_0^*) and the distance r from Tx at (0,0) to M.

We introduce the following definitions: $c_2 = v \cdot t_2 = r + r_2$ $c_4 = v \cdot t_4 = r + r_4$.

Consider triangles Tx-*M*-Rx2 and Tx-*M*-Rx4. Their areas (S) are equal because $S = ah/2$, where h is the common height of triangles Rx2-*M*-Tx and Rx4-*M*-Tx [with Tx at (0,0)]. The areas of these two triangles can also be found using Heron's formula

$$S_{\text{Tx}-M-\text{Rx2}} = \sqrt{p_2(p_2-a)(p_2-r)(p_2-r_2)} \tag{4}$$

$$S_{\text{Tx}-M-\text{Rx4}} = \sqrt{p_4(p_4-a)(p_4-r)(p_4-r_4)} \tag{5}$$

where p_2 and p_4 are the corresponding semiperimeters of the above-defined triangles with

$$p_2 = (c_2 + a)/2; \quad \text{and } p_4 = (c_4 + a)/2 \tag{6}$$

respectively. Equating RHS of (4) and (5) we obtain the equation for r

$$(c_2^2 - a^2)(a^2 - (c_2 - 2r)^2) = (c_4^2 - a^2)(a^2 - (c_4 - 2r)^2). \tag{7}$$

Algebra yields

$$a^2\frac{c_2^2-c_4^2}{c_4^2-a^2}-(c_2-2r)^2\frac{c_2^2-a^2}{c_4^2-a^2}+(c_4-2r)^2=0. \quad (8)$$

We can define s as

$$s=c_4-2r. \quad (9)$$

Substituting (9) into (8) yields the quadratic equation in s

$$(c_2+c_4)s^2+2\left(c_2^2-a^2\right)s+c_2\left(c_2^2-2a^2-c_2c_4\right)=0 \quad (10)$$

solutions of which are

$$s_\pm=\frac{-\left(c_2^2-a^2\right)\pm\left(a^2+c_2c_4\right)}{c_2+c_4} \quad (11)$$

or

$$s_+=\frac{2a^2-c_2^2+c_2c_4}{c_2+c_4},\quad s_-=-c_2. \quad (12)$$

We can find r using (9)

$$r_+=\frac{c_2^2+c_4^2-2a^2}{2(c_2+c_4)},\quad r_-=\frac{c_2+c_4}{2}. \quad (13)$$

As $a\to 0$, then $r_+\to r$ and $r_-\to 2r$. So, the only physically correct solution is for r_+. Thus, the distance r to the object is

$$r=r_+=\frac{v^2\left(t_2^2+t_4^2\right)-2a^2}{2v(t_2+t_4)}. \quad (14)$$

In the next step, we can find the coordinates for the object. Substituting (6) into (4) and (5) and equating these, we obtain

$$\frac{ah}{2}=\frac{1}{4}\sqrt{\left(c_2^2-a^2\right)\left(a^2-(c_2-2r)^2\right)}. \quad (15)$$

From (15), we can solve for the triangle height h

$$h=\frac{\sqrt{\left(c_2^2-a^2\right)\left(a^2-(c_2-2r)^2\right)}}{2a}. \quad (16)$$

From Fig. 2, $y_0^*=h$.

The x_0 coordinate of the object is found based on the relations

$$x_0=\sqrt{r^2-h^2}=\sqrt{r^2-\left(y_0^*\right)^2},\quad (c_2<c_4)$$
$$x_0=-\sqrt{r^2-h^2}=-\sqrt{r^2-\left(y_0^*\right)^2},\quad (c_2>c_4). \quad (17)$$

Thus, the distance r from the origin of the coordinate system to the object M at (x_0, y_0^*) can be found with the formulae

$$r=\frac{v^2\left(t_2^2+t_4^2\right)-2a^2}{2v(t_2+t_4)} \quad (18)$$

$$y_0^*=\frac{\sqrt{\left(v^2t_2^2-a^2\right)\left(a^2-(vt_2-2r)^2\right)}}{2a} \quad (19)$$

$$x_0=\sqrt{r^2-\left(y_0^*\right)^2},\quad (t_2<t_4)$$
$$x_0=-\sqrt{r^2-\left(y_0^*\right)^2},\quad (t_2>t_4). \quad (20)$$

These are the formulae for calculation of true coordinate x_0 and distance from Tx (origin) to the object r.

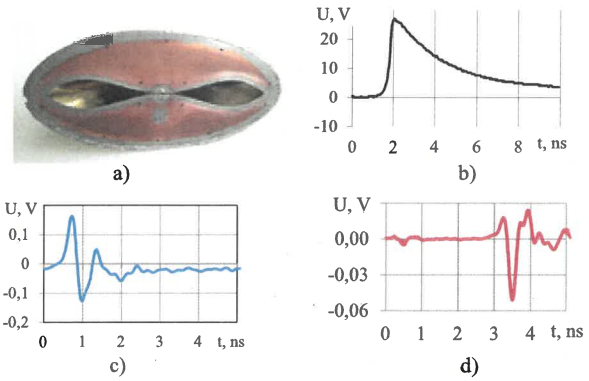

Fig. 3. (a) Shaped slot in elliptical metal plate, (b) exciting impulse of the generator at a load of 50 Ω, (c) direct coupling signal between Tx and Rx antennae, and (d) signal reflected by a metal sheet located at distance 50 cm from the antenna system.

B. Solution in the Plane Rx1-M-Rx3

A similar approach is used to calculate the distance r from the origin of the coordinate system at Tx to the object M at (x_0^*, y_0) where x_0^* may not be equal to x_0 because this plane is similarly non-horizontal. In this plane, the y coordinate is y_0 in the local reference system defined in Fig. 1.

This plane contains Tx, Rx1, Rx3, and M. In this plane, Rx1 and Rx3 are symmetrical with respect to the origin at a distance a [see Fig. 2(b)]. The geometrical definitions and mathematical procedure for this plane are analogous to those in Section III-A, with the goal being to determine the object coordinates (x_0^*, y_0) and distance r in this plane from the origin to the object M.

As for the prior plane, we define $c_1 = v\cdot t_1 = r + r_1$ $c_3 = v\cdot t_3 = r + r_3$, with the common height of the triangles Tx-M-Rx1 and Tx-M-Rx3 given by $S = ad/2$, with d as shown in Fig. 3.

The areas of these two triangles can also be found using Heron's formula

$$S_{\text{Tx}-M-\text{Rx1}}=\sqrt{p_1(p_1-a)(p_1-r)(p_1-r_1)} \quad (21)$$
$$S_{\text{Tx}-M-\text{Rx3}}=\sqrt{p_3(p_3-a)(p_3-r)(p_3-r_3)} \quad (22)$$

where p_1 and p_3 are the corresponding semi-perimeters of the triangles Tx-M-Rx1 and Tx-M-Rx3, with

$$p_1=(c_1+a)/2;\quad \text{and } p_3=(c_3+a)/2 \quad (23)$$

respectively. Equating RHS of (21) and (22), we obtain

$$\left(c_1^2-a^2\right)\left(a^2-(c_1-2r)^2\right)=\left(c_3^2-a^2\right)\left(a^2-(c_3-2r)^2\right). \quad (24)$$

This rearranges to

$$a^2\frac{c_1^2-c_3^2}{c_3^2-a^2}-(c_1-2r)^2\frac{c_1^2-a^2}{c_3^2-a^2}+(c_3-2r)^2=0. \quad (25)$$

We can define d as

$$d=c_3-2r. \quad (26)$$

After substitution of (26) into (25) and (24) and equating these two, we obtain the quadratic equation with respect to a variable d

$$(c_1+c_3)d^2+2\left(c_1^2-a^2\right)d+c_1\left(c_1^2-2a^2-c_1c_3\right)=0 \quad (27)$$

solutions of which are

$$d_\pm=\frac{-\left(c_1^2-a^2\right)\pm(a^2+c_1c_3)}{c_1+c_3} \quad (28)$$

or

$$d_+=\frac{2a^2-c_1^2+c_1c_3}{c_1+c_3},\quad d_-=-c_1. \quad (29)$$

Equation (26) yields r

$$r_+=\frac{c_1^2+c_3^2-2a^2}{2(c_1+c_3)},\quad r_-=\frac{c_1+c_3}{2}. \quad (30)$$

As $a\to 0$, then $r_+\to r$ and $r_-\to 2r$. So, the only physically correct solution is for r_+. Thus, the distance r to the object is

$$r=r_+=\frac{v^2\left(t_1^2+t_3^2\right)-2a^2}{2v(t_1+t_3)}. \quad (31)$$

Substituting (23) into (21) and (22) and equating these (similar to Section B, but following Fig. 3) yields the x_0^* coordinate of the object as

$$x_0^*=\pm d=\pm\frac{\sqrt{\left(c_1^2-a^2\right)\left(a^2-(c_1-2r)^2\right)}}{2a}. \quad (32)$$

The y_0 coordinate of interest is the positive value given by

$$y_0=\sqrt{r^2-d^2}=\sqrt{r^2-\left(x_0^*\right)^2},\quad (c_1<c_3). \quad (33)$$

The distance r from the origin to M and the coordinates (x_0^*, y_0) are given by

$$r=\frac{v^2\left(t_1^2+t_3^2\right)-2a^2}{2v(t_1+t_3)} \quad (34)$$

$$x_0^*=\frac{\sqrt{\left(v^2t_1^2-a^2\right)\left(a^2-(vt_1-2r)^2\right)}}{2a} \quad (35)$$

$$y_0=\sqrt{r^2-\left(x_0^*\right)^2},\quad (t_1<t_3). \quad (36)$$

Given the constraint (2), the condition $t_3>t_1$ is always valid and only the positive solution to (36) is considered.

C. 3-D Solution

Using the results of Sections III-A and III-B for the 2-D cases, we obtained the coordinates x_0 and y_0 for target M. Moreover, in both cases, we determined the distance r from the origin of the local coordinate system to the object M. Because it is truly the same object in both cases, the values of r must be equal for the two calculations. Thus, it is possible to calculate the vertical coordinate z_0 of the object M using the formula

$$r^2=x_0^2+y_0^2+z_0^2. \quad (37)$$

So

$$z_0=\sqrt{r^2-x_0^2-y_0^2}. \quad (38)$$

The sign of z_0 follows from condition (3).

Thus, using TOFs t_1, t_2, t_3, and t_4 measured by the 1 Tx + 4 Rx antenna system, we can get all three coordinates of the bright spot reflection from the object using formulae (20), (36), and (38).

IV. TOFs' Determination

To implement this algorithm, it is necessary to determine the TOFs for each of the receiver antennae Rx1–Rx4. One possible method is to use Pearson's correlation [15]. As described in [16], this method makes it possible to identify the object reflection in the recorded A-scans for each Rx antenna.

The definition of the TOF for a UWB radar is the delay between the transmitted and received pulses, with the latter representing the former as reflected by a remote target at a certain distance.

The estimation of the TOF must overcome problems posed by precision constraints that may be comparable to the pulse duration itself. Due to error propagation in the mathematical formulae, for even a coarse target positioning, a precise TOF estimation is required.

The basic idea is to estimate the time lag between a reference signal S_{REF} and the received signal S_{RX} and to use it for TOF calculation.

The reference signal S_{REF} is obtained by the reflection from a target at known distance D_{REF} for a certain known propagation velocity v_{REF}.

The TOF of the reference signal is known

$$\mathrm{TOF}_{\mathrm{REF}}=\frac{2\cdot D_{\mathrm{REF}}}{v_{\mathrm{REF}}}. \quad (39)$$

The lag defined by the delay between the signal received from the target S_{TGT} and the signal received from the reference S_{REF} is

$$\mathrm{LAG}=\mathrm{TOF}_{\mathrm{TGT}}-\mathrm{TOF}_{\mathrm{REF}}. \quad (40)$$

The lag can be estimated using a function F that is maximum when the reference signal, delayed by a time τ, correlates well with the received signal, and thus,

$$\mathrm{LAG}=\arg\max_{\tau}\{F[S_{\mathrm{REF}}(t-\tau), S_{\mathrm{RX}}(t)]\}. \quad (41)$$

The function F used for this article is the absolute value of Pearson's correlation [15] between the two signals $S_{\mathrm{RX}}(t)$ and $S_{\mathrm{REF}}(t-\tau)$.

The TOF of the target is thus given by

$$\mathrm{TOF}_{\mathrm{TGT}}=\mathrm{LAG}+\mathrm{TOF}_{\mathrm{REF}}=\mathrm{LAG}+\frac{2\cdot D_{\mathrm{REF}}}{v_{\mathrm{REF}}}. \quad (42)$$

V. Experimental Data and Analysis

For the validation of this algorithm, a preliminary set of experiments based on the 1 Tx + 4 Rx antenna system [12] with upgraded impulse GPR "ODYAG" [18] (Fig. 4) were carried out in laboratory. The results of this set of experiments were presented in [13] which show that a metal target of 10 cm diameter and 4 cm height was correctly detected on a 30 cm × 30 cm quadrant, and the positions located with an error less than the object radius of 5 cm. These results

Fig. 4. Target descriptions. (Top) Metal tin of 10 cm diameter and PMN-2 plastic landmine 12 cm diameter.

motivated testing of a realistic scenario for landmine detection, an outdoor experiment with buried metal and plastic targets in natural soil.

For this set of experiments, we used an upgraded 1 Tx + 4 Rx antenna system. As it was before [9], [12] the base of the antenna is a shaped slot in an elliptical metal plate [Fig. 3(a)]. The transmitting antenna dimensions are 1.5 times increased ($186 \times 90 \times 50$ mm^3). This creates a more powerful sounding impulse. The receiving antennas are shielded by a cone of metal (like the transmitting antenna). All antennas are placed on the same plane so that the E-field of Tx is directed at an angle of 45° to Rx1 and Rx3 and −45° to Rx2 and Rx4 (Fig. 5). The distances between the center of the transmitting antenna element and the centers of the four receiving antennae in the *xoy* plane are $a = 10$ cm.

The transmitting antenna is excited by a triangular impulse of voltage [Fig. 3(b)]. It induces the direct coupling signal [Fig. 3(c)] at the output of the receiving antennas. Reflection from a metal sheet located at a distance of 50 cm is shown in Fig. 3(d). The spatial characteristics of the antennas are similar to those presented in [9].

The antennae and the UWB pulse are designed with very short duration (0.3 ns) to achieve high-range resolution. The theoretical limit to range resolution corresponding to this duration for an impulse radar is 4.5 cm. Antenna switching for four positions provided sequential connection of the GPR receiver to all Rx1–Rx4 receiving antenna elements. The experimental setup and the discussion of results are reported in Section V-A.

A. TOF Measurement Setup

The targets selected for the outdoor experiment were a metal tin of 10 cm diameter and an inert plastic-cased landmine (PMN-2) with 12 cm diameter. In Fig. 4 (top) are shown the two targets on the natural ground before burial.

In Fig. 4 (bottom), we can observe the internal complexity of the plastic landmine with several mechanical components that make the electromagnetic response more complex than for the symmetrical cylindrical tin target.

The ground in the field in front of the Institute for Radiophysics and Electronics in Kharkiv is covered by short grass growing in clay-rich soil (see Fig. 4). During testing, the air temperature was +17 °C, and the snow had melted 4 weeks prior, leaving the ground still damp.

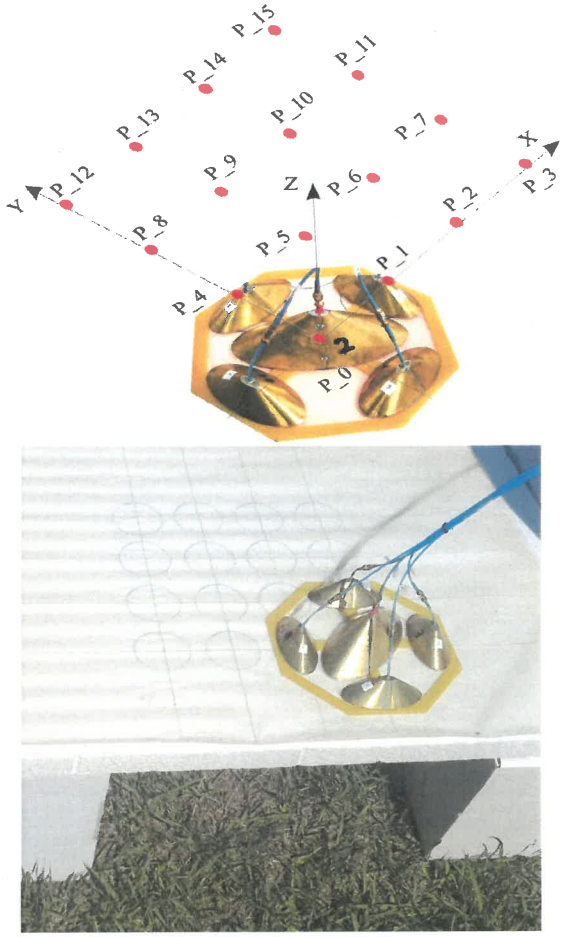

Fig. 5. Outdoor experimental set up. (Top) Grid of 6 × 5 antenna positions drawn on Styrofoam sheet. (Bottom) Antenna position in the origin of the X–Y coordinate system for the background signal acquisition. Antenna height from the ground is about 30 cm. The receiving antennas RX1 and RX3 are aligned on the OY-axis, while RX2 and RX4 are aligned on the OX-axis.

The data acquisition was made with similar setup as the previous experiments [13] to compare the detection and positioning performance. The antenna system was placed on Styrofoam blocks of 5 cm thickness at an approximate height of 34 cm over the ground (Fig. 5). At the beginning, we recorded the background signals for all four Rx antennas, with "background" meaning that no objects were in the ground for these measurements. The background measurements were acquired first and stored for further processing on all nodes of the 4 × 4 grid (see Fig. 5) covering an area of 30 cm × 30 cm as shown in Fig. 6.

Next, for the target detection experiment, the targets were buried a few centimeters in the damp clay soil corresponding to the position ($X = 0$, $Y = 0$, $Z = -34$ cm). Then, the antenna system was placed sequentially at the nodes of the grid, numbered P_0–P_15. At each position, we recorded the signals from each of the Rx1–Rx4 antennae. Precise alignment of the antenna system was facilitated by a red string crosshair (see Fig. 7).

The radar acquisition unit was set with 10-ps sampling time for the recorded signal and 16-bit analog-to-digital converter resolution.

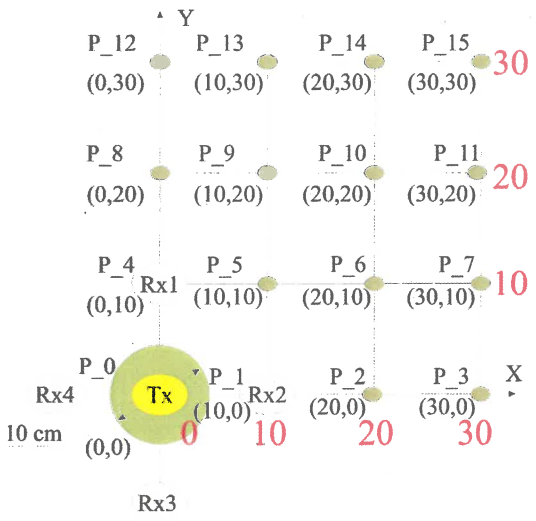

Fig. 6. Square grid of positions of the antenna (P_0–P_15) in the experimental reference system (see also Fig. 5). Unit of measure for (X, Y) coordinates is cm. Circle of diameter 10 cm corresponds to the projection of the target on the plane $Z = 0$.

Fig. 7. Alignment of the buried target with origin of the antenna position P_0.

B. Dependence of the Waveform of Reflected Signals on Distance and Angle of Illumination

Because the transmitting and receiving antennae are in proximity, there is still quite strong direct electromagnetic coupling between them. Therefore, to get only signals reflected by the object, we applied a procedure for subtraction of the background signal, including direct coupling, for each receiver from the signal recorded when the object was placed on the grid with a buried target. After the background removal, an example of the acquired signals (A-scans) for the four receiving channels RX1–RX4 is shown in Fig. 8 for two antenna positions P_0 and P_1.

The experimental data show that the reflected signals have different shapes and amplitude depending on the distance to the metal tin and on the angle of illumination relative to the scattering center of the target for each receiving antenna. In particular, in Fig. 8 (top) we can observe that after the negative peak at about 0.7 ns from the residual of the direct coupling signal from the Tx to each receiving antenna, the set of four signals acquired from symmetric positions (same

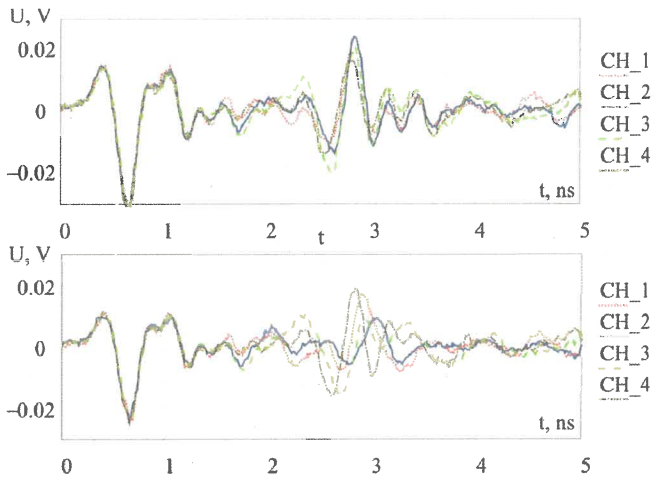

Fig. 8. A-scans for Rx1–Rx4 after background removal. (Top) Antenna position P_0 corresponding to the origin of the X–Y scanning plane. (Bottom) Antenna position P_1. Horizontal time scale t is [ns]. Vertical amplitude U scale is [volt].

distance and illumination angle) of the receiving antennae are very similar. Moreover, at about 2.7 ns, the four positive peaks reveal the sign inversion of the electric field on the metal surface and the differential TOF of $(2.8 - 0.7 + 0.3)$ [ns] $*$ 30 [cm/ns] $= 72$ cm. This empirical estimation was made to quickly verify that the signals are consistent with the theoretical travel path in air calculated as $(34 + 35.4)$ [cm] $=$ 69.4 cm, considering the center of the metal tin at ($X = 0$, $Y = 0$, $Z = -34$) cm.

A small amplitude (U) variation in the direct coupling signal from P_0 and P_1 can be observed and is due to a time shift of the UWB radar with temperature; however, this residual signal remains always well-separated from the reflected signals and has little influence on the following TOF estimations. In addition, a small difference in the shape and amplitude of the four pulses can be explained by the fabrication tolerances of the antenna system, or a slight non-horizontal tilt to the top of the tin target (i.e., slight variation in soil cover thickness).

Fig. 8 (bottom) shows the set of four received signals with the antenna at grid node P_1. In this example, RX4 (dot-dashed line) occupies position P_0 and then corresponds to the shortest TOF, as demonstrated by the experimental signals, while RX1 (dotted line) and RX3 (dashed line) have the same geometrical path length and the corresponding signals have the same TOF. Finally, the longer travel path is shown by the greatest TOF for RX2 (continuous line). Moreover, as expected, the amplitudes of the peaks decrease according to the increase in the path length (and therefore attenuation) depending on the receiving antenna positions.

The next step in our procedure is determining the TOFs for input to the location algorithm. To use the Pearson's correlation method described in Section IV, we need a digital sampling of the signal waveform that contains the reflection from the object. Considering the variation in waveforms (see Fig. 8), we decided to use a reference waveform obtained from a metal sheet located at a distance of 30 cm from the antenna system. A reference signal length of 150 samples (1.5 ns) was chosen (see Fig. 9).

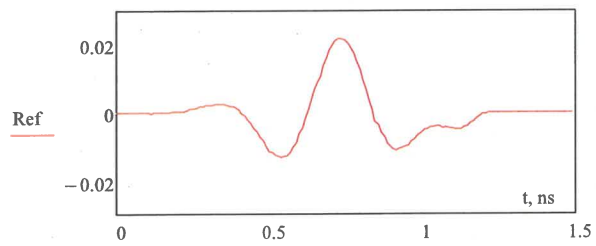

Fig. 9. Reference signal for cross correlation processing.

C. Coordinates of the Targets

For the next step of data processing, we analyzed all possible combinations of TOFs from Rx1 with Rx3, and Rx2 with Rx4. Using formulas (20), (36), and (38) we calculated feasible coordinates for the object (based on the three conditions in Section II). If the considered reflections correspond to the same object, the distance r must be the same in both planes of interest (Rx2-*M*-Rx4 and Rx1-*M*-Rx3). This is a criterion for arranging pairs of measurement results in the two planes. Note that the Zx coordinate is the depth coordinate Z calculated based on the data from the Rx2 and Rx4 plane, while the Zy coordinate is Z based on the data from the Rx1 and Rx3 plane. The averaged coordinates $z = (z_x + z_y)/2$ were used as a result.

Some of the combinations of the TOFs lead to unfeasible imaginary coordinates, immediately reducing the number of valid combinations. However, there are still many sets of physically possible coordinates: for 16 positions we obtained 52 set of possible coordinates for the metal object and 87 sets of coordinates for the plastic object.

At this stage of work, we have not yet developed an automatic algorithm to choose the "true" coordinates of the object. However, to determine whether the 1 Tx + 4 Rx antenna system yields accurate coordinates for the object, the obtained data are enough. Because we know all coordinates of the object in all positions, we can check whether the true coordinates or close-to-true coordinates exist in the corresponding sets. To account for the different signal-to-noise ratio, the threshold for Pearson's correlation is adjusted and set equal 0.2 for the metal tin and 0.1 for the plastic landmine. A visual representation of the results is shown in Fig. 10.

D. Discussion of Results

Regarding the metal tin, we found that the target is always detected. All target positions are detected, but only four are incorrectly located, being outside the target footprint (indicated with arrows in Fig. 10). In all other positions, the target location is correctly within the metal tin diameter. Regarding the plastic landmine, only three target positions are missed (P_12, P_13, and P_15) and half are detected incorrectly. However, for both cases, we can say that acceptable performances (no missed target) and precise positioning (i.e., within the diameter) are obtained in a full quadrant area of 20 cm × 20 cm; this result is consistent with that observed in the laboratory experiments [13].

It is also of interest to note the accuracy estimation for these experiments. Table I below lists the positioning errors for the

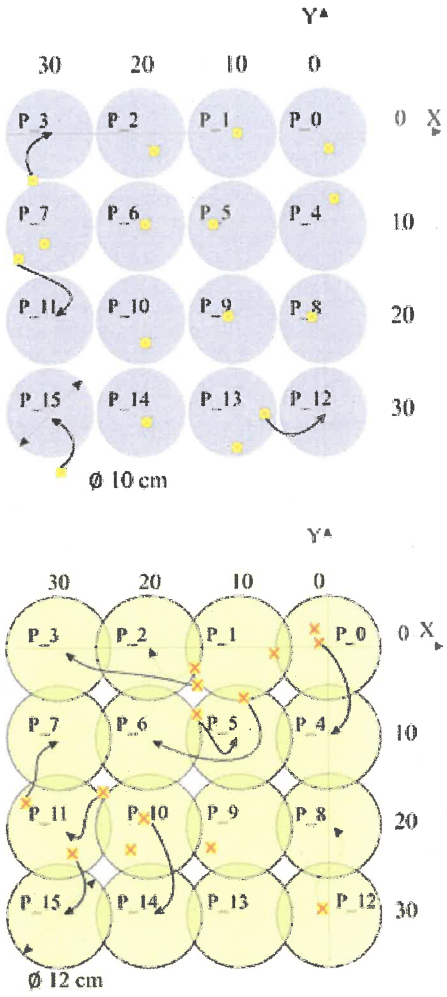

Fig. 10. Calculated positions of the two targets. (Top) Metal tin 10 cm diameter (blue circles). (Bottom) Plastic landmine 12 cm diameter (green circles). X–Y scale axes are in centimeter and origin P_0 on top and right corner.

metal target calculated as the distance from the GPR location to the nearest edge of the target footprint in the xy plane. Empty cells in Table I mean that the calculated position is inside the contour of the object. As we can see, the errors in positioning of the metal object are quite small (on the order of few centimeters) and are much less than the diameter of the metal target.

The results are not as good for the plastic target. There are two detected positions P_12 and P_13 with the corresponding errors almost two times larger than the target diameter. Assuming the worst case, this means that in these positions the objects are missed. However, it is important to remember that the robotic platform is moving, so the target should be detected as it moves to another position in the grid.

As is evident in Fig. 10, if the metal target is located right under the antenna system, then the detected coordinates are usually very close to the center. While if the target is located outside of the antenna array footprint, the coordinates of the detected position tend to shift onto the side of the cylindrical target facing the array.

If we consider the signal path geometry sketched in Fig. 11, there is a possible explanation of this phenomenon—which

TABLE I
POSITIONING ERRORS IN CENTIMETERS

	Metal				PMN-2			
P_N	x	y	z	Err	x	y	z	Err
0								
1								
2								
3	-31.9	-5	-33.5	0.35	-14.40	-4.10	-34.2	10.13
4					-1.00	0.50	-32.3	4.55
5								
6					-9.20	-6.60	-25.2	5.32
7					-33.70	-17.30	-38.7	2.18
8					-0.70	-29.30	-35.1	3.33
9								
10								
11	-34	-13	-35.3	3.06	-25.00	-16.10	-37.8	0.34
12	-6.5	-30.2	-35.6	1.50	0.00	-2.80		21.20
13					-38.30	-20.20		23.95
14					-20.50	-19.10	-39.1	4.91
15	-28.5	-37.6	-28.7	2.75	-28.50	-23.00	-37	1.16

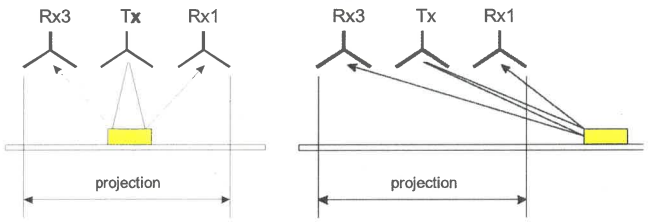

Fig. 11. (Left) Path for reflection of the transmitted impulse if the object is located under the antenna elements and (Right) if the object is located out of projection of the circle containing the antenna array.

was also observed in the experiments reported in [13]. In the target positions P_0, P_1, P_4, and P_5 (see Fig. 6), reflections come mostly from the top surface of the object. In this case, the detected coordinates are very close to the top center of the object and the radar cross section (RCS) is high. However, if the object is located outside of the projection of the array footprint (see right image in Fig. 11), the side surface of the targets may produce the brightest reflection, and the detected positions move away from the center of the object. This can be observed in Fig. 10 for positions far from origin at P_0. For the plastic landmine target, the electromagnetic response is even more complicated due to the response of the internal parts that modify the waveform of the reflected signal. This behavior was studied systematically by the MIMEVA project [19] for several landmines. An angular dependence of the RCS for the targets placed just outside the array footprint can be considered to improve the precision of positioning.

VI. CONCLUSION

On the basis of a simple model and experiments, the possibility of using the 1 Tx + 4 Rx antenna system and UWB impulse GPR to detect a mine-like object and determine its Cartesian coordinates has been demonstrated. The dimensions of the mine-like object are equivalent to the spatial duration of the pulse, which does not allow us to consider the object as a point target. The detection of the object and determination of its coordinates are performed in the near zone of the antenna system, which necessitates the use of an object coordinate determination algorithm based on measuring the TOFs of the probing signal from the transmitter to the object and then to each of the receiving antennae.

The design of the antenna system, in which the transmitting antenna is in the center and four receiving antennas are in the corners of a square (with a radius of circumference of 10 cm), as well as its geometrical parameters, made it possible to obtain simple relations for calculating all three Cartesian coordinates for the object using four TOFs. Because the real objects are not point targets, the TOFs and the coordinates correspond to the bright spot or strongest reflecting area.

In this article, an algorithm based on the calculation of the Pearson's correlation coefficients is applied to determine the TOFs, allowing determination, with sufficient precision, the arrival time of the reflected pulse. However, the presence of the interfering rereflections of the probing signal in the received signal as well as the nonidentical form of the signals scattered by the object from different angles led to the presence of several possible values of the TOF and the need to develop an algorithm for selecting true TOFs [13].

It was found that among the combinations of TOFs that determine the distance from the object to each of the receiving antennae, there is a set of coordinates corresponding to the location of the object. Moreover, in all cases, the buried plastic landmine and metal tin targets were detected, and the calculated targets position falls in most cases within the object diameter achieving the successful detection and location of a shallow target. We also observe the rather remarkable success for the plastic mine—getting 50% correct locations in a real scenario where damp clay soil often renders GPR useless, and the transparency of a plastic case plus internal structure adds complication.

It was shown by the field experiments that the task of determining the coordinates is solved in the left upper quadrant of the coordinate system with a scanning region size of 30 cm × 30 cm. Hence, the total size of the surveyed area would be at least 60 cm × 60 cm for a real survey. This area is quite large for the survey of a lane in humanitarian demining applications.

This antenna system has also been used in experiments on detection of plastic mine simulants buried in natural ground when mounted on a robotic vehicle achieving similar performances, with the results of this work described in [20].

In general, these results demonstrate the capability and accuracy of the 1 Tx + 4 Rx antenna system. Automatic determination of unambiguous TOFs by identification of true reflections from the target will be solved in the next steps of research. Using a single reference signal to calculate the correlation is probably too simple, and an adaptive reference signal could be calculated to compensate for soil conditions and UWB GPR electronics jitter with time.

In the future, an extensive campaign of experiments on different targets in varied soil types will reveal the statistical detection performances based on the receiver operating characteristic (ROC) analysis across multiple tests.

REFERENCES

[1] E. Colon *et al.*, "An integrated robotic system for antipersonnel mines detection," *Control Eng. Pract.*, vol. 10, no. 11, pp. 1283–1291, 2002.

[2] J. M. Gibson, R. Harmon, J. MacDonald, J. R. Lockwood, J. E. McFee, J. S. Ashwood, T. Altshuler, T. Broach, and L. Carin, *Alternatives for Landmine Detection*. Santa Monica, CA, USA: RAND, 2003.

[3] M. K. Habib, "Humanitarian demining: Reality and the challenge of technology—The state of the arts," *Int. J. Adv. Robot. Syst.*, vol. 4, no. 2, p. 19, 2007.

[4] P. F. Santana, J. Barata, and L. Correia, "Sustainable robots for humanitarian demining," *Int. J. Adv. Robot. Syst.*, vol. 4, no. 2, pp. 206–218, 2007.

[5] M. K. Habib, "Development of robot and navigation techniques for humanitarian demining," in *Proc. 6th IEEE Int. Conf. Ind. Inform.*, Daejeon, South Korea, Jul. 2008, pp. 418–423. doi: 10.1109/INDIN.2008.4618135.

[6] S. Havlik, "Land robotic vehicles for demining," in *Humanitarian Demining*, M. K. Habib, Ed. Rijeka, Croatia: InTech, 2008, ch. 13. [Online]. Available: http://www.intechopen.com/books/humanitarian_demining/land_robotic_vehicles_for_demining

[7] I. Arezzini, M. Calzolai, L. Lombardi, L. Capineri, and Y. Kansal, "Robotic system for detection of shallow buried objects," in *Proc. Prog. Electromagn. Res. Symp.*, Kuala Lumpur, Malaysia, Mar. 2012, pp. 1207–1211.

[8] L. Capineri *et al.*, "High resolution imaging with a holographic radar mounted on a robotic scanner," in *Proc. PIERS*, Stockholm, Sweden, Aug. 2013, pp. 1583–1585.

[9] G. Pochanin *et al.*, "Design and simulation of a 'single transmitter—Four receiver' impulse GPR for detection of buried landmines," in *Proc. 9th Int. Workshop Adv. Ground Penetrating Radar (IWAGPR)*, Jun. 2017, pp. 1–5.

[10] C. Windsor, L. Capineri, and T. D. Bechtel, "Buried object classification using holographic radar," *Insight-Non-Destructive Test. Condition Monit.*, vol. 54, no. 6, pp. 331–339, 2012.

[11] T. Bechtel, L. Capineri, C. Windsor, M. Inagaki, and S. Ivashov, "Comparison of ROC curves for landmine detection by holographic radar with ROC data from other methods," in *Proc. 8th Int. Workshop Adv. Ground Penetrating Radar (IWAGPR)*, Jul. 2015, pp. 1–4.

[12] O. Pochanin *et al.*, "Estimation of lane width for object detection using impulse GPR with '1Tx and 4Rx' antenna system," in *Proc. 17th Int. Conf. Ground Penetrating Radar (GPR)*, Rapperswil, Switzerland, Jun. 2018, pp. 1–5.

[13] T. Ogurtsova *et al.*, "Criteria for selecting object coordinates at probing by the impulse UWB GPR with the '1Tx + 4Rx' antenna system," in *Proc. 9th Int. Conf. Ultrawideband Ultrashort Impulse Signals (UWBUSIS)*, Odessa, Ukraine, Sep. 2018, pp. 161–164.

[14] D. J. Daniels, "Ground penetrating radar for buried landmine and IED detection," in *Unexploded Ordnance Detection and Mitigation* (NATO Science for Peace and Security Series B: Physics and Biophysics), J. Byrnes, Ed. Dordrecht, The Netherlands: Springer, 2009, pp. 89–111.

[15] K. Pearson, "Notes on regression and inheritance in the case of two parents," *Proc. Roy. Soc. London*, vol. 58, pp. 240–242, Jun. 1895.

[16] C. G. Windsor and L. Capineri, "Automated object positioning from ground penetrating radar images," in *Proc. INSIGHT*, 1998, vol. 40, no. 7, pp. 482–488.

[17] J. S. Bendat and A. G. Piersol, *Engineering Applications of Correlation and Spectral Analysis*. New York, NY, USA: Wiley, 1993, p. 458.

[18] G. P. Pochanin *et al.*, "Advances in short-range distance and permittivity ground-penetrating radar measurements for road surface surveying," *Advanced Ultrawideband Radar: Signals, Targets, and Applications*, J. D. Taylor, Ed. Boca Raton, FL, USA: CRC Press, 2016, ch. 2, pp. 19–64.

[19] European Commission, DG Joint Research Centre Institute for Systems, Informatics and Safety Technologies for Detection and Positioning Unit TP, Varese, Italy. *Project MIMEVA: Study of generic Mine-like Objects for R&D in Systems for Humanitarian Demining—Final Report Prepared for DG Information Society (DG INFSO) Unit E-6 Contract Reference (Administrative Agreement): AA 501852*. [Online]. Available: https://www.gichd.org/fileadmin/pdf/LIMA/MIMEVA.pdf

[20] G. Pochanin *et al.*, "Application of the industry 4.0 paradigm to the design of a UWB radiolocation system for humanitarian demining," in *Proc. UWBUSIS*, Odessa, Ukraine, Sep. 2018, pp. 50–56. doi: 10.1109/UWBUSIS.2018.8520226.

Gennadiy P. Pochanin (M'97–SM'07) was born in Kharkov, Ukraine, in June 9, 1961. He received the M.Sc. and Ph.D. degrees in radiophysics and electronics from Kharkov State University, Kharkov, in 1983 and 2003, respectively.

Since 1985, he has been a Scientist with the Institute for Radiophysics and Electronics of the National Academy of Sciences of Ukraine (IRE NASU), Kharkov, where he is currently a Chief of the Radiophysical Introscopy Department. He has coauthored six books, more than 60 articles, and more than 10 inventions. His current research interests include transient wave phenomena, radiation and reception of ultrawideband short pulses of electromagnetic waves, ultrawideband antennas, ultrawideband radars, and ground-penetrating radars.

Dr. Pochanin is a winner of the State Prize of Ukraine in the area of Science and Technology 2016. He received the Senior Researcher Academic Status in 2005.

Lorenzo Capineri (M'83–SM'07) was born in Florence, Italy, in 1962. He received the M.S. degree in processing method for ground-penetrating radar systems from the University of Florence, Florence, in 1994.

In 1995, he became an Associate Researcher and an Associate Professor of Electronics with the Department of Information Engineering, University of Florence, in 2004. In 2017, he received the National Scientific Qualification as a Full Professor in electronics. He has worked on several research projects in collaboration with national industries, the Italian Research Council (CNR), the Italian Space Agency (ASI), and the European Space Agency (ESA), AEA Technology and UKAEA, England, International Science and Technology Centre (ISTC), Moscow, Russia, Thales Alenia Space Italia (TASI), Texas Instruments, USA, Joint Research Centre (European Commission), and North Atlantic Treaty Organization (NATO). He has coauthored three book chapters and more than 200 scientific and technical articles. He holds six Italian patents. His current research interests include the design of ultrasonic guided wave devices, buried objects' detection with seismo-acoustic methods, and holographic radar.

Timothy D. Bechtel (M'08) was born in Summit, NJ, USA, in 1961. He received the B.Sc. degree in geology from Haverford College, Haverford, PA, USA, and the M.Sc. degree in rock mechanics and the Ph.D. degree in geophysics from Brown University, Providence, RI, USA.

He has been a Contract Geophysicist with Enviroscan, Inc., Lancaster, PA, USA, and several previous firms gaining 30 years of experience in UXO detection and mapping. He has taught geophysics, geocomputation, and engineering geology at the University of Pennsylvania, Philadelphia, PA, USA, and environmental geology, hydrogeology, and geophysics at the Franklin and Marshall College, Lancaster, PA, USA, where he is currently a Teaching Professor and the Director of Science Outreach. His current research interests include UXO detection and discrimination, and hydrogeophysics and remote sensing for characterizing karst aquifers and alpine peat lands.

P. Falorni, photograph and biography not available at the time of publication.

Giovanni Borgioli was born in Florence, Italy, in 1949. He received the Laurea degree in physics with the University of Florence, Florence, Italy, in 1974.

Since 2010, he worked on mathematical models for acoustic and radar signal processing for landmine detection. He was appointed as an Associate Professor of rational mechanics with the Politecnico di Torino, Turin, Italy, in 1987, and in 1990, he returned to the Engineering Faculty, University of Florence, joining the Department of Electronics and Telecommunications. He is currently with the Department of Mathematics and Informatics U. Dini, University of Florence. His current research interests include heat diffusion, neutron transport, kinetic theory, and quantum transport.

Vadym P. Ruban (M'07) was born in Ukraine in 1979. He received the Dipl.-Ing. Degree in radiophysics engineering from V.N. Karazin Kharkiv National University, in 2002.

Since 2002, he has been a Junior Researcher with the Radiophysical Introscopy Department, O.Ya. Usikov Institute for Radiophysics and Electronics of the National Academy of Science of Ukraine, Kharkiv, Ukraine. He has coauthored one book, more than 15 articles, and 1 invention. His current research interests include ground-penetrating radar designing, receiving, and processing of the impulse UWB signals.

Oleksandr A. Orlenko was born in Kharkiv, Ukraine, in 1974. He received the degree in radiophysics engineering from V. N. Karazin Kharkiv National University, in 1996.

Since 1999, he has been a Junior Researcher with the Radiophysical Introscopy Department, O.Ya. Usikov Institute for Radiophysics and Electronics of the National Academy of Science of Ukraine, Kharkiv. He has coauthored 10 articles. His current research interests include design and performance short pulse generators, multielement antenna systems, and antenna measurement techniques.

Tetiana M. Ogurtsova was born in Poltava, Ukraine, in 1967. She received the Dipl.-Ing. degree with the Faculty of Mechanics and Mathematics, Kharkov State University, Kharkov, Ukraine, in 1989.

Since 1989, she has been a Junior Researcher with the Radiophysical Introscophy Department, O.Ya. Usikov Institute for Radiophysics and Electronics of the National Academy of Science of Ukraine, Kharkov. She has coauthored more than 5 articles, 1 invention, and 12 conference articles. Her current research interests include computer modeling of the parameters of the UWB antennas and GPR data processing.

Oleksandr G. Pochanin was born in Kaliningrad, Russia, in 1983. He received the Dipl.-Ing. degree with the Faculty of Mechanics and Mathematics, V.N. Karazin Kharkiv National University, in 2004.

Since 2004, he has been a Software Engineer with the Radiophysical Introscopy Department, O.Ya. Usikov Institute for Radiophysics and Electronics of the National Academy of Science of Ukraine, Kharkiv. Since 2016, he has been a Software Engineer in private companies. He has coauthored more than one book, 5 articles, and 8 conference articles. His current research interests include UWB ground-penetrating radar data processing.

Fronefield Crawford was born in Bryn Mawr, PA, USA in 1972. He received the B.A. degree in astrophysics from the Williams College, Williamstown, MA, USA, and the Ph.D. degree in physics from MIT, Cambridge, MA, USA.

He teaches courses in physics and astronomy at the Franklin and Marshall College, Lancaster, PA, USA, where he is currently a Professor with Astronomy and Director of Grundy Observatory. He was previously employed as a Senior Systems Engineer with Lockheed Martin, King of Prussia, PA, USA, where he worked on remote sensing systems. His current research interests include the study of radio pulsars using large radio telescopes, the search for low-frequency gravitational waves using pulsars as detectors, and the detection and identification of landmines using remote sensing methods.

P. Kholod, photograph and biography not available at the time of publication.

L. Bossi was born in Prato, Italy, in 1973. He received the M.S. degree in electronic engineering from the University of Florence, Florence, Italy, in 2018, where he is currently pursuing the Ph.D. degree in information engineering.

He served compulsory military service as a Soldier in 1995. He has owned a business and worked as an Entrepreneur. From 2017 to 2018, he was a Research Fellow with the Department of Information Engineering, University of Florence, where he developed algorithms to improve the quality of information contained in microwave subsurface holographic radar images. He worked on research projects in collaboration with North Atlantic Treaty Organization (NATO) SPS. He has coauthored more than three articles. He has worked on diagnostic systems for wooden structures and cultural heritage infested from xilophagous insects. His current research interests include microwaves, penetrating radars, robotic platforms with sensors integration, nondestructive testing.